スピン軌道トルクを用いた反強磁性/強磁性ヘテロ構造の制御とその不揮発メモリ、脳型情報処理応用

博士学位論文要約（平成30年３月）

スピン軌道トルクを用いた反強磁性/強磁性ヘテロ構造の制御とその不揮発メモリ、脳型情報処理応用

クレンコフ アレクサンダー

指導教員：大野 英男，　研究指導教員：深見 俊輔

Spin-orbit torque controlled antiferromagnet/ferromagnet heterostructures for nonvolatile memory and neuromorphic computing

Aleksandr Kurenkov

Supervisor: Hideo Ohno,　Research Advisor: Shunsuke Fukami

I study spin-orbit torque induced magnetization switching in devices consisting of an antiferromagnetic PtMn and ferromagnetic Co/Ni multilayer with sizes ranging from 5 μm to 50 nm. As the size decreases, switching behavior changes from analogue-like to stepwise with several intermediate levels. The number of intermediate levels decreases with the decreasing size and finally evolves into a binary mode below a certain threshold. The results are explained by individual reversal of ferromagnetic domains comprising a number of polycrystalline grains. I also study high-frequency properties of the system and find that pulses from 1 s to 1 ns and their sequences can be used for magnetization reversal. I explain features of this switching by temperature dynamics in the system.

1. Introduction

Spin-orbit torque (SOT) induced magnetization switching [1,2] is a promising technology for writing information in three-terminal spintronic memory devices. Such configuration offers higher reliability and faster operation speed (by pulses down to 180 ps [3]) than conventional two-terminal counterparts. Most of the studies have focused on the switching in nonmagnet (NM)/ferromagnet (FM)/metal oxide heterostructures in which SOT mainly originates from spin Hall effect of the NM and/or the Rashba effect at the interface of FM. In such stacks, rotational symmetry of Slonczewski-like component of SOT must be broken to achieve bidirectional switching. Application of external in-plane magnetic field is a possible solution, but more technologically applicable methods for breaking the symmetry are required. Such a method is to use antiferromagnets (AFMs). They can exert exchange bias (EB) on adjacent FMs and it can effectively replace the required in-plane field. In addition, it has been shown that some of them exhibit inverse/direct SHE and can, therefore, generate spin currents. Recent study has combined these two effects to demonstrate field-free switching in AFM/FM bilayer structure. Interestingly, switching in this case is analogue-like (or “memristive”), i.e. it is not binary and its degree can be controlled by adjusting pulse amplitudes [4]. To apply these findings to binary or analogue AFM/FM memory cells, it is important to clarify the mechanism governing the observed magnetization reversal mode. To do it, in this work I study size-dependent properties of AFM/FM heterostructures, operated by SOT [5].

Another direction of this study is high-frequency operation of AFM/FM devices. Up to now, studies involving SOT switching in AFM/FM had been done with direct current despite the high-speed potential of the approach. Here I extend functionality of AFM/FM memristors and binary devices to high-frequency domain by using pulses from 1 s to 1 ns for switching. I also find that magnetization state can be reproducibly controlled by application of trains of pulses which allows non-trivial single-device implementations such as counters or registers. Analysis of temperature evolution in the device allows me to explain dependence of switching current on pulse width.

2. Device fabrication and measurements

Stacks of Ta(3)/ Pt(4)/ $Pt_{40}Mn_{60}$(9)/ [Co(0.3)/ Ni(0.6)]$_2$/ Co(0.3)/ MgO(1.2)/ Ru(1) (thicknesses are in nm; the PtMn composition is that of the sputtering target) were deposited on highly resistive Si wafers by dc/rf magnetron sputtering. They were patterned into circular dots consisting of a Co/Ni multilayer on top of the Ta/Pt/PtMn channel with Hall probes by electron beam lithography and Ar ion milling (Fig. 1).

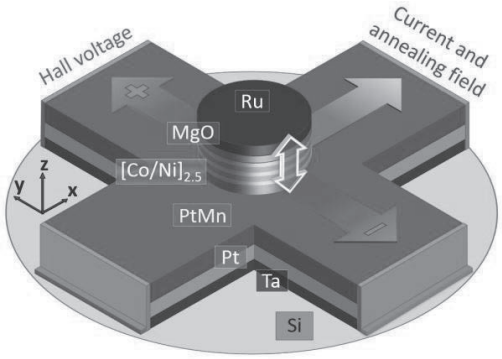

Figure 1. Schematic diagram of the fabricated dot devices with a coordinate system, measurement scheme and exchange bias direction.

Cr(5)/Au(100) electrodes were formed at the ends of the channel and Hall probes to provide contacts for electrical measurements. The fabricated devices were subsequently annealed at 300°C for two hours in the presence of the 1.2T magnetic field, directed along the X axis, to provide EB. Figure 1 shows a schematic diagram of patterned devices. I varied dot diameter (D_{dot}) with 25-nm increment and fabricated at least 15 devices of each size and stack structure. The channel width W_{ch} was 150, 500, or 1100 nm depending on D_{dot}. The same fabrication procedure without a dot patterning process was used to fabricate Hall bar devices with the 5x15-μm^2 channel. The measurement procedure was as follows. First, magnetization was initialized in the -Z direction by the positive dc current with sufficient amplitude I_{INI}. This was followed by sweeping 100-ms-long channel current I_{ch} pulses in the direction 0 → -I_{MAX} → +I_{INI} → 0. This sequence was repeated for various I_{MAX} to examine magnetization reversal with various intermediate levels. Magnetization state was probed by measuring anomalous Hall resistance R_{Hall} after each pulse with 100 μA dc current, small enough not to perturb magnetization state. All measurements were performed at room temperature.

3. Origin of memristive switching

Figures 2(a)–2(f) show R_{Hall}–I_{ch} curves, measured at zero fields for devices from 5 μm to 50 nm. Memristive behavior in Hall bars (Fig. 2(a)) changes to a step-wise loop with a series of intermediate resistance levels, and the number of the intermediate levels progressively decreases with the device size reduction (Fig. 2(b)–2(e)). Finally, below 225 nm, we observe binary

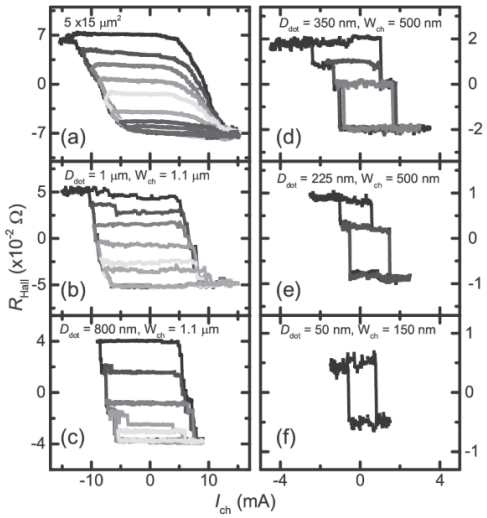

Figure 2. Size-dependent field-free SOT switching (R_{Hall}-I_{ch} loops) for devices of various sizes: (a) 5-μm Hall bar, (b) D_{dot} = 1 μm, (c) D_{dot} = 800 nm, (d) D_{dot} = 350 nm, (e) D_{dot} = 225 nm and (f) D_{dot} = 50 nm.

reproducible switching, while field- free magnetization reversal is conserved even in the smallest 50nm dots (Fig. 2(f)). I also note that variation of the shape of R_{Hall}–I_{ch} curves is smaller for larger devices. Switching current density, J_{SW}, defined as a mean of current densities in PtMn at which R_{Hall} jumps, is around 2×10^{11}A/m^2 and is virtually independent of device size. This contrasts with previous research on NM/FM heterostructures, which shows binary switching even in μm-sized Hall bars and significant variation in J_{SW} with device size. This implies a different mechanism of magnetization reversal in the present AFM/FM system. It is schematically shown in Fig. 3b, in which each device consists of a number of domains with different properties, which switch separately in response to the applied current.

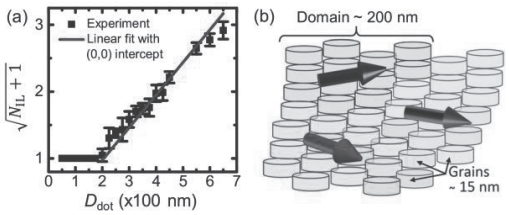

Figure 3. (a) Dot size dependence of number of intermediate states (red line is linear fit). (b) Schematics illustrating possible reversal mechanism.

Analogue-like switching of larger devices even in the process of magnetization reversal by magnetic field (R_{Hall}-H_Z loops) and alternation of this switching by application of in-plane H_X magnetic field allow to determine variation of exchange bias between the domains as a reason for their nonsimultaneous switching and, therefore, memristive behavior. Consequently, it is determined by AFM which explains why magnetization reversal process is so different from conventional NM/FM systems.

Next, I estimate mean diameter of ferromagnetic domains from the observed hysteresis loops. The switching mode and intermediate states show no noticeable change over multiple cycles of measurements, indicating that the observed behavior is related to domain structures inherent to each device. Assuming that the field or current switches each domain individually, one can estimate domain period from the number of intermediate levels (N_{IL}) that should reflect the number of domains accommodated in a dot. Such analysis for devices that have distinguishable intermediate states is shown in Fig. 3(a) and according linear fit gives domain diameter of 205±7 nm. This is much larger than the estimated by transmission electron microscopy grain size of 15 nm, which refines the picture of switching, shown in Fig. 3(b). Hence, each FM domain with a certain direction of EB must consist of several AFM grains.

4. Properties of ultrafast switching

In this chapter, I investigate switching of PtMn/[Co/Ni] Hall bars by pulses of different widths τ_p. I applied a positive pulse of sufficient amplitude and certain τ_p to initialize a Hall bar. Then I applied rectangular switching pulses with current densities j_{ch} sweeping from zero to negative and then to positive direction (as in Chapter 3), but with the chosen pulse width τ_p. The obtained R_{Hall}-j_{ch} hysteresis loops for different τ_p (Fig. 4) provide evidence that pulses from 1 s to 1 ns can perform reliable memristive switching.

Figure 5 summarizes these properties for single pulses of different amplitudes and widths. For each point of the phase diagram I initialize the device by magnetic field before applying a pulse of desired parameters. One can see that it is possible to control the device state by adjusting not only pulse amplitude, but also pulse width. This is due to nonlinear dependence of switching current on pulse width. As it becomes smaller then ~ 20 μs, switching current starts to increase rapidly. I explain this dependence by

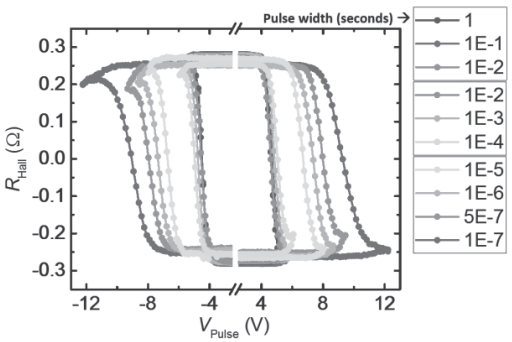

Figure 4. Memristive hysteresis loops for pulses of different widths.

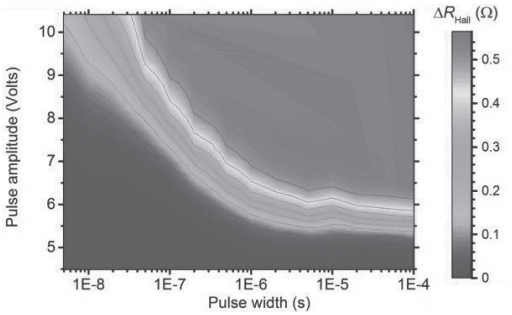

Figure 5. Phase diagram of switching by pulses of different widths and amplitudes.

lack of Jole heat, generated by shorter pulses. It increases temperature of the samples, which promotes magnetization reversal. To estimate temperature dynamics, I compare change of sample resistance under a current pulse with dependence of resistance on the temperature of the sample. The result is shown in Fig. 6. Temperature saturates in approximately 20 μs which explains the trend observed in Fig. 5. It is an evidence that heat, generated by current pulses is crucial for high-speed SOT switching in AFM/FM

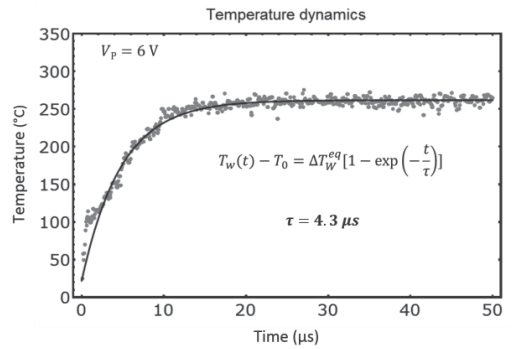

Figure 6. Temperature dynamics with exponential fit.

systems and must be considered accordingly by designing thermal parameters of the devices. This is done through changing the parameter τ (4.3 μs in this case), which is inherent to the system and can be used to calculate temperature evolution under application of arbitrary pulses.

5. Conclusions

This work clarifies different aspects of SOT switching in AFM/FM heterostructures. On the one hand, it explains why in such systems unconventional memristive switching is observed and how the switching mode can be controlled. On the other hand, it shows that pulses as short as 1 ns can be used to control magnetization state. Additional studies have demonstrated that sequential application of identical pulses can continuously alter the state of an AFM/FM device. This rich variety of options for switching behavior (binary, stepwise, memristive) and control methods (by pulse amplitude, pulse width, number of pulses) in combination with speed and robustness of SOT switching, allows applications in binary and analogue-like memory devices as well as in perspective nontrivial devices such as counters, registers and integrators. Moreover, it is promising for applications in biologically inspired computing, such as recently shown associative memory in an artificial neural network [6].

References

[1] I. M. Miron *et al.*, Perpendicular switching of a single ferromagnetic layer induced by in-plane current injection. Nature **476**, 189–193 (2011).
[2] L. Liu *et at.*, Spin-torque switching with the giant spin Hall effect of tantalum. Science **336**, 555 (2012);
[3] K. Garello *et al.*, Ultrafast magnetization switching by spin-orbit torques. Appl. Phys. Lett. **105**, 212402 (2014).
[4] S. Fukami, C. Zhang, S. DuttaGupta, A. Kurenkov and H. Ohno, Magnetization switching by spin–orbit torque in an antiferromagnet–ferromagnet bilayer system. Nat. Mater. **15**, 535 (2016).
[5] A. Kurenkov, C. Zhang, S. DuttaGupta, S. Fukami and H. Ohno, Device-size dependence of field-free spin-orbit torque induced magnetization switching in antiferromagnet/ferromagnet structures. Appl. Phys. Lett. **110**, 092410 (2017).
[6] W. A. Borders *et. al.*, Analogue spin–orbit torque device for artificial-neural-network-based associative memory operation. Appl. Phys. Express **10**, 013007 (2017).